Electron-capture cross sections of multiply charged slow ions of carbon, nitrogen, and oxygen in He

K. Ishii,[1] A. Itoh,[1] and K. Okuno[2]
[1]*Quantum Science and Engineering Center, Kyoto University, Kyoto 606-8501, Japan*
[2]*Department of Physics, Tokyo Metropolitan University, Minami-Ohsawa, Tokyo 192-0397, Japan*
(Received 10 June 2004; published 25 October 2004)

Experimental cross sections are presented for single- and double-electron capture by C^{q+}, N^{q+}, and O^{q+} ($q=2-6$) ions from He at incident energies of $(1.0-1800)q$ eV. Measurements were performed by using a mini-electron-beam-ion-source apparatus in combination with an octopole-ion-beam-guide. The cross sections are found to vary significantly depending on the collision energy as well as on the projectile species. Some cross sections reveal minima at incident energies of a few eV/u, below which the cross sections increase with decreasing incident energy. To account for the experimental results, we developed a formalism of velocity-dependent capture cross sections within the framework of the classical over barrier model by employing an induced dipole interaction potential between the collision partners. In the calculations, doubly excited levels of projectile ions, formed via simultaneous excitation of the outermost projectile electron, were taken into consideration. It is found that the present model can satisfactorily reproduce the experimentally obtained energy dependence as well as absolute values of the cross sections. We conclude that the attractive induced dipole potential and simultaneous projectile excitation are important in low energy electron-capture collisions.

DOI: 10.1103/PhysRevA.70.042716 PACS number(s): 34.70+e

I. INTRODUCTION

Electron-capture cross sections of multiply charged slow ions in collisions with atoms and molecules are fundamental data in atomic physics and of practical importance in various application fields. In particular, cross sections involving C^{q+}, N^{q+}, and O^{q+} ions have received increasing attention in plasma physics, astrophysics and thermonuclear fusion researches. To date, a number of experimental and theoretical studies have been carried out for various multiply charged slow ions, and summarized data tables are available in the literature [1,2].

It is known that electron-capture cross sections of highly charged ions with keV/u energies do not depend greatly on the collision energy and are nearly the same order of magnitudes irrespective of the projectile species when the incident charges q are the same. Hence, considerable efforts have been devoted to developing simple scaling formulas in terms of q and I, the target ionization potential. Müller and Salzborn [3] proposed a well-known scaling formula, $\sigma = Aq^{\alpha}I^{\beta}$, using empirically determined scaling parameters A, α, and β, which has been widely applied for one- through four-electron capture cross sections of various highly charged ions.

Since electron capture by slow ions is essentially state-selective, cross sections measured at relatively low charge states often reveal q oscillations when plotted as a function of q [4]. Such characteristics are not derived from the scaling formula given above, but have been successfully reproduced by the classical overbarrier (COB) model [4,5]. Bárány *et al.* [6] and Niehaus [7] extended this model to multiple electron-capture processes including transfer ionization as well in a highly sophisticated way of calculation procedure. Besides these classical models, a number of quantum mechanical calculations have been made so far, although they are limited to single-capture cross sections [8]. Olson and his co-workers formulated the multichannel Landau-Zener (MCLZ) calculations using empirical nonadiabatic transition probabilities [9,10].

Contrary to numerous experimental data obtained above 1 keV/u, cross section data below keV/u are scarcely available until recently due to technical difficulties in producing low energy ion beams with sufficiently high intensities and narrower energy spreads. These difficulties may be overcome by using a multipole-beam-guide operated with RF voltages [11]. We employed an octopole ion beam guide (OPIG) and combined it with a well established mini-EBIS (electron beam ion source) apparatus. This combined technique enabled us to carry out successful measurements of charge-changing cross sections for various multiply charged slow ions [12–14]. Capture cross sections for multiple-electron targets of Ne, Ar, N_2, O_2, and CO were found to vary dramatically as a function of the collision energy, never showing a flat behavior as expected form the above scaling formula which contains no velocity-dependent term. That is, many cross sections exhibit minimum dips at about 1 eV/u and begin to increase with decreasing collision energy. This strong velocity-dependent behavior indicates obviously that a low-energy collision characteristic such as a Langevin type orbiting model [15] should be taken into consideration.

In this paper, we present a set of experimental cross section data for single- and double-electron capture by C^{q+}, N^{q+}, and O^{q+} ($q=2-6$) ions in a He gas target at collision energies below 1 keV/u. The experimental data are discussed in detail by comparing them with theoretical calculations by our newly developed COB model, in which an induced-dipole potential between collision partners [11,15] is taken into consideration in order to obtain velocity-dependent capture cross sections. The experimental values are also compared with MCLZ calculations based on the formalism developed by Salop and Olson [9].

II. CALCULATIONS

A. Calculations of the classical overbarrier model

In this section, we describe our calculation model, referred to as M(modified)COB hereafter, developed on the basis of the extended classical-overbarrier model formulated in [6,7]. Essentials of this model are given briefly and then our procedure is described.

In this model, a capture cross section of r-electrons by an A^{q+} ion from a target B with n_e electrons is calculated by

$$\sigma_{q,q-r} = \sum_j \sum_{t=1}^{t_{max}} P_t^{(j)} A_t, \tag{1}$$

where $A_t = \pi(b_{t,in}^2 - b_{t+1,in}^2)$ the ring-shaped geometrical cross section, $P_t^{(j)}$ the transfer probability associated with the tth target electron in a string (j), and t_{max} the smaller number of q and n_e, e.g., $t_{max}=2$ in the present collision systems. The impact parameter $b_{t,in}$ is determined from the critical nuclear distance $r_{t,in}$ in the "way-in," at which distance the perturbed binding energy of tth electron equals to a maximum potential barrier V_m formed by the collision partners,

$$-I_t - \frac{q}{r_{t,in}} = V_{m,in} = -\frac{1}{r_{t,in}}(\sqrt{q} + \sqrt{t})^2, \tag{2}$$

and we obtain

$$r_{t,in} = \frac{1}{I_t}(2\sqrt{qt} + t). \tag{3}$$

From the definition given above, $r_{t,in}$ corresponds to the classical turning point. Similarly, in the "way-out" condition, the critical distance $r_{t,out}$ is defined by the equation

$$-I_t - \frac{q}{r_{t,in}} = V_{m,out} = -\frac{1}{r_{t,out}}(\sqrt{q-k} + \sqrt{t+k})^2, \tag{4}$$

and consequently,

$$r_{t,out} = r_{t,in}\left(\frac{\sqrt{q-k} + \sqrt{t+k}}{\sqrt{q} + \sqrt{t}}\right)^2. \tag{5}$$

Here, it is assumed that inner k-electrons of the target are captured prior to the outer tth electron. In case of He, k is always 0 for the second electron $(t=2)$, and $k=1$ for the first electron $(t=1)$ in strings $j=(0,1)$ and (1, 1).

The electron binding energy is assumed to vary dynamically in time, and the mean values in the projectile and in the target frames are given respectively by

$$\varepsilon_{t,P} = I_t + \frac{q}{r_{t,in}} - \frac{t+k}{r_{t,out}}, \tag{6}$$

$$\varepsilon_{t,T} = I_t + \frac{q}{r_{t,in}} - \frac{q-k}{r_{t,out}}. \tag{7}$$

The energy spread of these binding energies (energy window) is given by a Gaussian distribution function,

$$F_t(\varepsilon) = (\Delta\varepsilon_t \pi^{1/2})^{-1} \exp\left[-\left(\frac{\varepsilon - \varepsilon_t}{\Delta\varepsilon_t}\right)^2\right], \tag{8}$$

where ε_t stands for the energy of either projectile (P) or target (T) in Eqs. (6) and (7). The width $\Delta\varepsilon_t$ is obtained from the uncertainty of the potential barrier height ΔV_m given by

$$\Delta V_m = \left|\frac{dV_m}{dr} v_r\right|^{1/2}. \tag{9}$$

As there are two values of ΔV_m in the way-in $(r=r_{t,in})$ and way-out $(r=r_{t,out})$, $\Delta\varepsilon_t$ is obtained by

$$\Delta\varepsilon_t = (\Delta V_{m,in}^2 + \Delta V_{m,out}^2)^{1/2}. \tag{10}$$

The transition probability ω_t of the tth electron is calculated using statistical weights of two states expressed in Eqs. (6) and (7). About more details of this extended-COB model, readers should refer to [7].

In our MCOB model, we start from the equation of motion described in the center-of-mass frame by

$$E_o = \frac{1}{2}\mu v_r^2 + \frac{b^2}{r^2}E_o + V(r), \tag{11}$$

where μ is the reduced mass, $E_o = \mu v_o^2/2$ is the initial kinetic energy in the c.m. frame, v_r is the relative radial velocity, and b is the impact parameter. In low velocity collisions, the interaction potential $V(r)$ may be approximated by the induced dipole potential [15],

$$V(r) = -\frac{\alpha q^2}{2r^4}, \tag{12}$$

with α the polarizability of the target; $\alpha(\mathrm{He}) = 0.205$ (Å^3) $= 1.38$ a.u. The relationship between the classical turning point r_c and the corresponding impact parameter b_c is obtained from Eq. (11) by putting $v_r = 0$,

$$b_c = r_c\sqrt{1 - \frac{V(r_c)}{E_o}} = r_c\sqrt{1 + \left(\frac{r_{orb}}{r_c}\right)^4}, \tag{13}$$

where $r_{orb} = (\alpha q^2/2E_o)^{1/4}$ is the classical orbiting radius, inside this radius the incident particle begins to orbit towards the target center. The impact parameters $b_{t,in}$ in Eq. (1) are calculated from Eq. (13) by putting $r_c = r_{t,in}$. Note that the second term $V(r)/E_o$ is neglected in other COB models [5,7], and hence $b_t = r_t$ in their calculations. It should be pointed out that r_{orb} is velocity dependent and becomes large at low incident energies, while the values of $r_{t,in}$ are velocity independent. Here, if $r_{t,in} < r_{orb}$, then the geometrical cross section for the capture of tth electron should be replaced by the Langevin cross section, $\pi b_{orb}^2 = \pi\sqrt{2\alpha q^2/E_o}$, because the incident ion "orbiting" towards the target nucleus inevitably passes the point of $r_{t,in}$ during orbiting.

Also, it should be noted that, in many experimental studies on state-selective electron capture, the simultaneous excitation of projectile electron (electron promotion) is known to play an important role in electron-capture collisions [16–19]. Actually, some of our experimental capture cross sections can hardly be explained if this effect is not taken into consideration, as described in the following sections. We

include this process, occurring predominantly to the outermost projectile electron, within the framework of the COB model as follows. The transfer equation in this case is expressed by

$$-I_p - \frac{t_{max}}{r} = V_{m,p} = -\frac{1}{r}(\sqrt{q+1} + \sqrt{t_{max}})^2, \tag{14}$$

where I_p [$>I_2$(He)=54.4 eV] is the ionization potential of the outermost projectile electron, $q+1$ and $t_{max}=2$ are the core charges exerted to this electron. The nuclear distance satisfying the equation is obtained by

$$r_p = \frac{1}{I_p}(2\sqrt{(q+1)t_{max}} + q + 1), \tag{15}$$

and the corresponding impact parameter b_p is calculated from Eq. (13). Note that r_p is the same both in the way-in and way-out. The corresponding energy window, given by Eq. (8), is calculated with the mean binding energy $\varepsilon_p = I_p$ and the uncertainty of the potential barrier height is obtained by r differentiation of $V_{m,p}$. Note $r_p < r_{2,in}$ from the definition.

In this way, we introduce four nuclear distances of r_1, r_2, r_p, and r_{orb}. The transition probability w_t for the tth electron was calculated as follows. First, we used exact atomic level energies cited from NIST atomic energy database [20] in the energy window function $F(\varepsilon)$ instead of continuous values. This may be reasonably supported because, in our collision systems, the principal quantum numbers of relevant capturing states are limited to relatively low values (<4), and hence subshell separations are large compared to large n levels. Namely, we used the following values as the total weights of electronic states into which the electron is finally stabilized,

$$W = \sum_J F_t(\varepsilon_J)(2J+1), \tag{16}$$

where ε_J and $(2J+1)$ are the binding energy and the statistical weight of the state in the LS coupling scheme. The transition probability w_t is then calculated by

$$w_t = \frac{W_P}{W_P + W_T}, \tag{17}$$

with $W_{P,T}$ the total statistical weights corresponding to projectile (P) and target (T). Similarly, the promotion probability of the projectile electron is obtained by

$$w_p = \frac{\sum_p F_p(\varepsilon_p)}{\sum_p F(\varepsilon_p) + F_p(I_p)}, \tag{18}$$

with ε_p the doubly excited level energy.

The radial velocities $v_{r,t}$ used in Eq. (9) are calculated from Eq. (11) as

$$v_{r,t} = v_o\left(1 - \frac{\overline{b^2}}{r_t^2} + \frac{r_{orb}^4}{r_t^4}\right)^{1/2} = \frac{v_o}{r_t}(b_t^2 - \overline{b^2})^{1/2}. \tag{19}$$

Here, we used mean impact parameters $\overline{b^2}$ defined separately according to the order of rings, i.e., $\overline{b^2}$ for the ith ring is calculated by

$$\overline{b_i^2} = \frac{b_i^2 + b_{i+1}^2}{2}, \tag{20}$$

with $i=1,2,p,orb$ when $r_1 > r_2 > r_p > r_{orb}$, $i=1,orb$ when $r_1 > r_{orb} > r_2 > r_p$, and so forth. Here, $\overline{b_{orb}^2}$ is always put to $b_{orb}^2/2$ because b_{orb} is the geometrical radius for any reaction processes occurring inside.

Some examples of cross section calculations are given below.

Case 1: $j=(1,0)$, and $r_1 > r_2 > r_p > r_{orb}$

$$\sigma_{q,q-1} = \omega_1^{(1)}A_1 + \omega_1^{(2)}(1-\omega_2^{(2)})A_2 + [\omega_1^{(3)}(1-\omega_2^{(3)})(1-\omega_p) + \omega_{1p}^{(3)}(1-\omega_{2p}^{(3)})\omega_p]A_3 + \omega_{1p}^{(4)}(1-\omega_{2p}^{(4)})A_{orb}.$$

Here, ω_{tp} is the transition probability calculated using doubly-excited level energies, superfix (i) is the ring number, and $A_{orb} = \pi b_{orb}^2$. We assume $\omega_p = 1$ for $b \leqslant b_{orb}$.

Case 2: $j=(1,1)$ and $r_1 > r_2 > r_p > r_{orb}$,

$$\sigma_{q,q-2} = \omega_1^{(2)}\omega_2^{(2)}A_2 + [\omega_1^{(3)}\omega_2^{(3)}(1-\omega_p) + \omega_{1p}^{(3)}\omega_{2p}^{(3)}\omega_p]A_3 + \omega_{1p}^{(4)}\omega_{2p}^{(4)}A_{orb}.$$

Case 3: $j=(1,0)$ and $r_1 > r_2 > r_{orb} > r_p$,

$$\sigma_{q,q-1} = \omega_1^{(1)}A_1 + \omega_1^{(2)}(1-\omega_2^{(2)})A_2 + \omega_1^{(3)}(1-\omega_2^{(3)})A_{orb}.$$

Finally, we note the validity and limitation of the present model. As the attractive induced dipole potential of Eq. (12) may be accurate only at large nuclear distances, the present model becomes worse when the incident ion comes too close to the target. As a rough estimation, we took this critical distance as twice the displacement distance d of the dipole moment induced by the electric field of the incident ion, $ed \simeq \alpha q e/(2d)^2$, giving rise to $2d \simeq 1.8$ a.u. and 2.5 a.u. for $q=2$ and 6, respectively. The present model is considered to be valid when these critical distances are much smaller than the values of $r_{t,in}$ which, calulated from Eq. (3), are $r_{1,in}=4.2(q=2) \sim 6.5(q=6)$, and $r_{2,in}=3.0(2) \sim 4.5(6)$. These evaluations support safely the present model to be valid for single-capture cross sections, while the accuracy may be worse for double-capture processes. It is emphasized that the present model may be applied more successfully for more highly $(q>5)$ charged slow heavy ions.

B. Multichannel Landau-Zener model

The multichannel Landau-Zener calculations for single-electron-capture cross sections were carried out following the formalism by Olson and his co-workers [9,10]. In this model, the transition probability at the diabatic potential curve crossing r_c is given by

$$p = \exp\left(-\frac{2\pi H_{12}^2}{\Delta F v_r}\right), \tag{21}$$

where H_{12} is one half the adiabatic splitting at r_c and ΔF is the difference in slopes of the diabatic potential energy curves at r_c. Taulbjerg [21] improved the coupling matrix element H_{12} as expressed by

$$H_{12} = \frac{9.13 f_{nl}}{\sqrt{q}} \exp\left(\frac{-1.324\sqrt{2I_t}}{\sqrt{q}} r_c\right), \tag{22}$$

with

$$f_{nl} = (-1)^{n+l-1}(2l+1)^{1/2}\Gamma(n)[\Gamma(n+l+1)\Gamma(n-l)]^{-1/2}, \tag{23}$$

where I the ionization potential of the target, and nl is the final projectile state where the electron is captured. In our calculations, we again use the induced dipole potential and the curve crossing distance r_c at which initial and final diabatic potential energies equal to each other was obtained by the following equation:

$$-\frac{\alpha q^2}{2r_c^4} - I_1 = \frac{(q-1)}{r_c} - \varepsilon_{nl}, \tag{24}$$

where ε_{nl} is the binding energy of the nl state [20]. In order to obtain more accurate cross sections, we also included channels of doubly excited states in addition to singly excited states. The radial velocity v_r in Eq. (21) was calculated from Eq. (11) at the position $r=r_c$.

When there are N crossings in total, the transition probability P_i into the ith level is calculated by

$$P_i = p_1 p_2 \cdots p_i(1-p_i)[1 + (1-p_{i+1})^2 + p_{i+1}^2(1-p_{i+2})^2 + \cdots + p_{i+1}^2 p_{i+2}^2 \cdots p_{N-1}^2(1-p_N)^2 + p_{i+1}^2 p_{i+2}^2 \cdots p_N^2], \tag{25}$$

and the capture cross section is obtained by b integration as

$$\sigma_{q,q-1} = 2\pi \sum_i^N \int_0^\infty P_i b \, db. \tag{26}$$

III. EXPERIMENT

The experiment was performed using the mini-EBIS atomic collision facility of Tokyo Metropolitan University. Figure 1 shows a schematic diagram of our experimental setup. The experimental procedure has been described in detail elsewhere [22], so that only a brief outline is given below. Projectile ions extracted from the mini-EBIS were mass-separated by an electromagnet analyzer (MS1) and decelerated before entering an OPIG which works also as a target gas cell. After collisions with a He target, outgoing projectile ions were accelerated again and then their mass and charge were separated by the second electromagnetic analyzer (MS2). The energy spread of the primary beam was about 1.0 eV/q at FWHM. The collision energy was determined by the potential difference between the ion source and the OPIG collision cell. Single and double electron-capture cross sections were measured at He gas pressures below 1×10^{-2} Pa, being low enough to ensure single collisions. Experimental errors of the cross sections are ±30% at most.

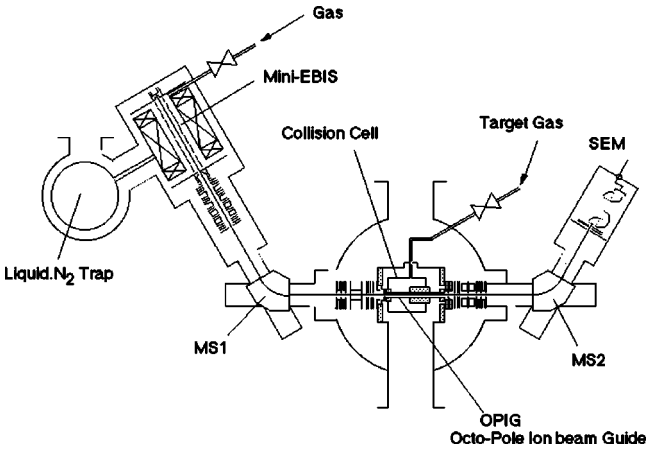

FIG. 1. Schematic diagram of experimental setup.

We have routinely checked long-lying excited ions in the primary ion beam by means of a beam attenuation method [23]. The mini-EBIS was operated with a DC mode at a pressure below 10^{-8} Pa, so that practically no long-lying excited ions were produced via electron-capture collisions with residual gases inside the ion source [11]. It is noted that most long-lying excited ions, if any, may be quenched easily inside the ion source because the confinement time of about 1 ms is sufficiently long to quench such ions. Actually, we found no metastable ions in the primary beams except for C^{2+} and O^{2+}. The metastable fractions were found to be about 3% and 3.5% for these beams, respectively.

IV. RESULTS AND DISCUSSION

Experimental data for single- (σ_1) and double- (σ_2) electron-capture cross sections are summarized in Table I. The data are plotted in Figs. 2–4 together with other experimental and theoretical data obtained mostly at higher energies. Note here that the data below 0.5 eV/q are also shown in parentheses as references. As a whole, the present results can safely be connected with these high energy data. Present low energy data show that the incident energy dependence is considerably different for different charge states and different incident ion species. Some cross sections vary rapidly but others not, and some ones appear to increase below a few eV/u. These features are discussed in the following sections in comparison with our MCOB and MCLZ calculations.

Cross sections for $q=2-6$ are shown separately in Figs. 5–9. In the right-hand sides of these figures, corresponding energy window functions $F_t^{(j)}(\varepsilon)$, calculated at 100 eV/u as a demonstration, are also shown as a function of the electron binding energy ε. It is noted that central energies in strings $j=(0,1)$ and (1, 1) are the same, and $\varepsilon_{2,T}=I_2$ for all the strings. It should be kept in mind that when the binding energy of a certain electronic state lies within the energy window under consideration, the state is a possible candidate for electron capture.

TABLE I. Single- (σ_1) and double- (σ_2) electron-capture cross sections for C^{q+}, N^{q+}, and O^{q+} ($q=2-6$)+He. Units are in 10^{-16} cm^2.

		C^{q+}+He		N^{q+}+He		O^{q+}He	
q	Energy (eV/q)	σ_1	σ_2	σ_1	σ_2	σ_1	σ_2
$q=2$	1.0			1.1		0.96	
	2.0			1.1		0.90	
	5.0			1.4		1.7	
	10			2.6		2.7	
	20			5.1		3.7	
	50	0.93		9.8		5.8	
	70	1.7					
	100	1.7		11		5.8	
	140	2.2					
	200	3.1		13		7.4	
	300	2.8					
	500	5.9		12		11	
	700	6.1					
	1000	6.8		16		11	
	1500					8.7	
	1800	12		14		10	
$q=3$	(0.5)	(2.0)		(3.6)		(6.8)	(0.31)
	1.0	2.1		3.6	0.097	6.3	0.19
	2.0	2.1		4.0	0.095	4.7	0.085
	5.0	3.5		3.0	0.056	5.3	0.062
	10	6.0		2.8	0.038	4.2	0.052
	20	8.8		3.0	0.067	4.6	0.070
	30					5.8	0.12
	50	12		3.3	0.16	6.4	0.17
	70					7.5	0.17
	100	13		4.1	0.21	5.7	0.17
	200	10		3.9	0.18	5.4	0.26
	300					6.3	0.30
	500	9.3		4.9		5.4	0.31
	700					6.4	0.38
	1000	17	0.047	6.7	0.32	5.2	0.75
	1800	15	0.051		0.33	8.3	0.83
$q=4$	(0.5)					(3.4)	(0.31)
	1.0			0.87	0.66	3.1	0.31
	2.0			0.68	0.59	2.6	0.19
	5.0			0.59	0.57	2.6	0.10
	10		0.064	0.94	0.72	2.0	0.051
	20		0.090	1.3	0.95	1.7	0.082
	30		0.18				
	40		0.26				
	50		0.35	1.5	1.7	1.5	0.079
	70	0.075	0.73				
	100	0.17	1.4	1.6	1.9	2.0	0.14
	140	0.17	1.9				
	200	0.18	2.5	2.0	2.3	1.9	0.15
	300	0.20	3.2	4.0	3.9		
	500	0.24	3.9	4.1	2.9	2.2	0.35

TABLE I. (*Continued.*)

		$C^{q+}+He$		$N^{q+}+He$		$O^{q+}He$	
q	Energy (eV/q)	σ_1	σ_2	σ_1	σ_2	σ_1	σ_2
	700	0.30	4.3				
	1000	0.48	3.3	3.9	1.9	3.4	0.49
	1800	0.84	4.5	4.5		4.1	0.40
$q=5$	(0.5)	(11)	(0.52)	(7.7)	(0.17)	(15)	(0.80)
	1.0	10	0.58	7.6	0.16	14	0.64
	2.0	11	0.36	8.3	0.13	13	0.52
	5.0	17	0.083	12	0.088	14	0.20
	10	23		14	0.087	16	0.17
	15	19					
	20	27		20	0.26	20	0.33
	30	20					
	50	28	0.044	24	0.41	28	0.64
	100	34	0.11	24	0.61	31	1.0
	200	29	0.16	23	1.2	32	1.3
	500	27	0.27	24	2.7	34	1.9
	1000	30	0.24	23	2.5	32	1.7
	1800	26	0.42	25	2.4	29	1.9
$q=6$	(0.5)			(0.13)	(0.041)		
	1.0			0.11	0.032	0.069	0.073
	2.0			0.072	0.027	0.035	0.015
	3.0					0.016	0.0071
	4.0					0.024	0.013
	5.0			0.12	0.049	0.037	0.011
	7.0					0.039	0.024
	10			0.43	0.092	0.088	0.073
	15					0.14	0.16
	20			0.87	0.11	0.16	0.25
	30					0.24	0.24
	50	0.24	0.26	1.4	0.22	0.35	0.22
	100	0.49	0.60	2.2	0.37	1.1	0.36
	200	0.80	3.5	0.55	2.2	1.3	
	250	1.1					
	300					3.3	1.9
	350	2.2	0.64				
	500			5.2	0.61	3.8	2.0
	750	7.1	0.99				
	950	7.5	0.88				
	1000			7.5	0.88	9.9	3.5
	1500	7.3	1.1				
	1800			11	0.77		

For help in understanding our discussion, a general explanation is described at first using the N^{3+} data (Fig. 6) as an example. Experimental data of σ_1 and σ_2 are depicted by closed and open circles, respectively. The MCOB calculations for single- (SC) and double- (DC) electron capture are shown by solid lines and dotted lines, respectively. The MCLZ calculations are given by dashed lines with a label LZ. As for the MCOB calculations, curves labeled by NP are the results calculated without taking account of the electron-promotion and other curves include this process. All these notations are the same in other figures.

The MCOB calculations of SC can reproduce fairly well the experimental values of σ_1 which are nearly constant in the whole range of incident energy. It is noted that the calculated values "NP" are completely incorrect, indicating clearly that the electron promotion process plays an impor-

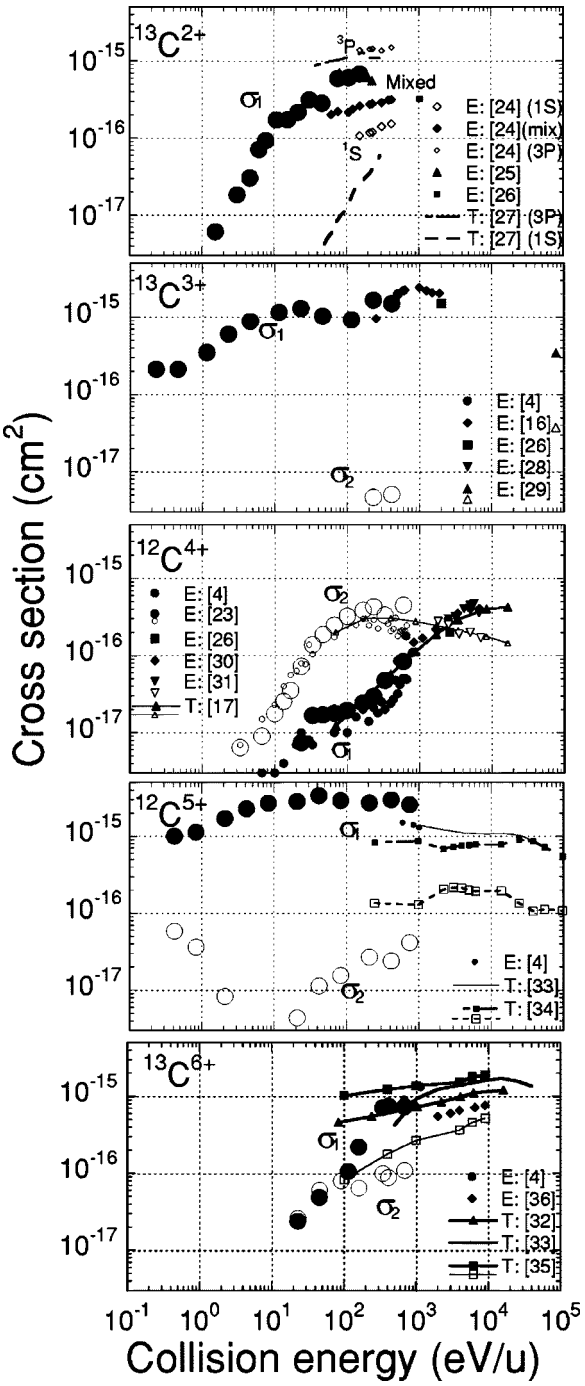

FIG. 2. Single- and double-electron-capture cross sections for $C^{q+}+He$ in comparison with other exdperimental (E) and theoretcial (T) data [4,16,17,23–36].

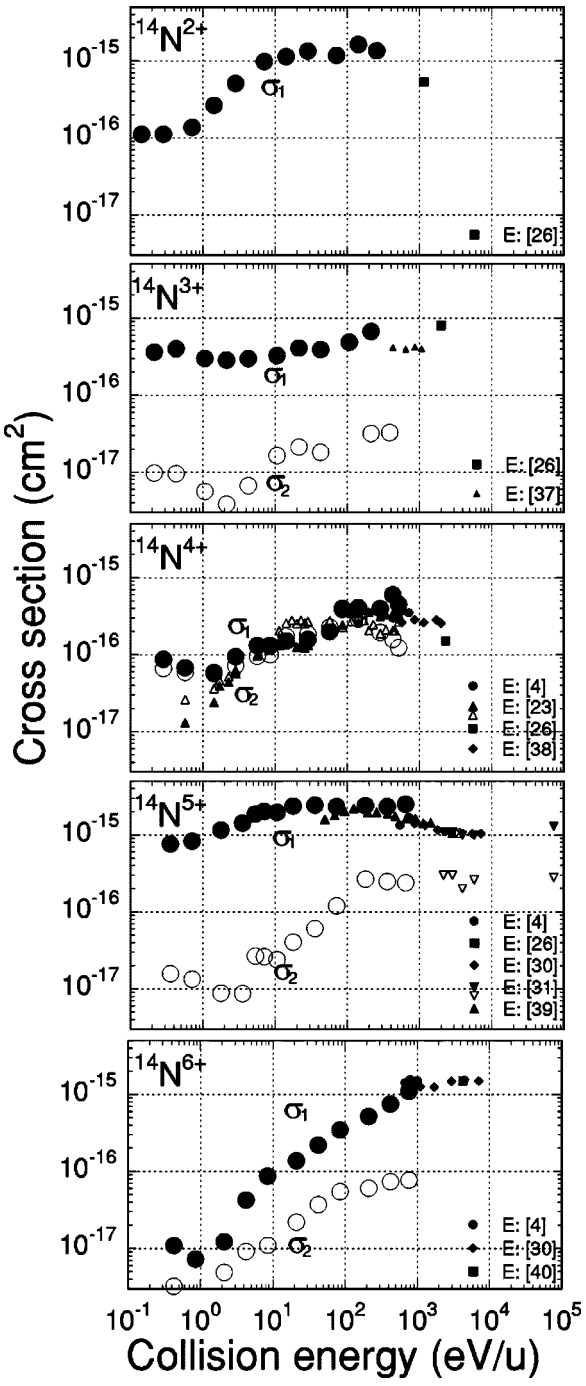

FIG. 3. Single- and double-electron-capture cross sections for $N^{q+}+He$ in comparison with other experimental (E) and theoretical (T) data [4,23,26,30,31,37–40].

tant role in electron-capture collisions. This can be understood qualitatively from the corresponding energy window spectra shown in the right-hand side of the figure. Namely, for the predominant single-capture process denoted by the string $j=(1,0)$, there exist no available capturing states in N^{2+}, while there are some doubly excited states lying within the energy window. Thus, if these doubly excited states are excluded, cross sections are calculated to be significantly small values at, in particular, low energies as shown by curves NP.

The MCOB cross sections reveal a dip at about 10 eV/u and increase with decreasing incident energy. This feature is attributed to the classical orbiting effect characterized by the Langevin cross sections σ_L shown by a dot-dashed line in the figure. However, such a dip structure is unclear experimentally.

The double-capture cross sections σ_2 are found to have a dip at about 2 eV/u and shows the Langevin type increase in the low energy region. By contrast, the MCOB calculations (DC) cannot reproduce this feature as well as the magnitude

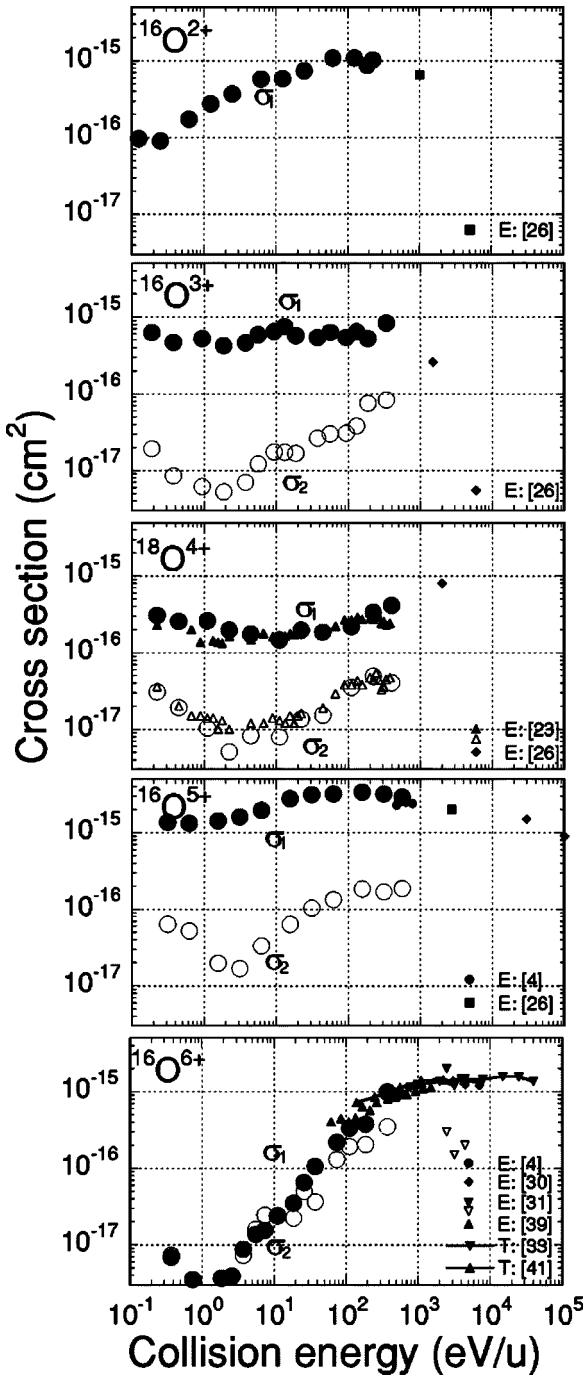

FIG. 4. Single- and double-electron-capture cross section for O^{q+}+He in comparison with other experimental (E) and theoretcial (T) data [4,23,26,30,31,33,39,41].

of the experimental cross sections. Theoretical values are more than one order of magnitudes larger than the experimental ones at higher energies (>100 eV/u) and drop rapidly in the low energy region. We speculate that this large discrepancy arises from inappropriate use of the energy width ($\Delta\varepsilon$) in the energy window functions. As $\Delta\varepsilon$ is roughly proportional to the incident ion velocity as $v_o^{1/2}$ [see Eqs. (9), (10), and (19)] the energy window $F_{2P}^{(j)}$ becomes wider enough to cover the ground state level of $N^{2+}(2s^2 2p)$ at higher incident energies. Consequently, the capture probability of the second electron of He may be overestimated in our calculations. Similarly at low incident energies, the energy window becomes narrower preventing the energy overlapping between the N^{2+} ground state and $F_{2P}^{(j)}$, resulting in rapid decrease of double-capture cross sections.

The MCLZ calculations were made by including also doubly excited states [20]. The results, shown by a dashed line, reveal a similar energy dependence as the MCOB results but are slightly larger than the latter. It is noted that the MCLZ model also predicts the Langevin type increase at low energies, which comes from the use of the induced dipole potential in our calculations.

A. C^{2+}, N^{2+}, and O^{2+}

Figure 5 shows the single-capture cross sections σ_1 for $q=2$. Electron capture by these A^{2+} ions is dominated by single-electron capture, and double-capture events are nearly absent experimentally. This is explained from similar level-overlap considerations given above. One can see that the energy window functions $F_{2P}^{(j)}$ are located far from the ground states of A^+ ions for all the ions, so that the capture probabilities of the second electron of He are negligibly small. Actually, the MCOB calculations show the DC cross sections to be more than three orders of magnitude smaller than the single-capture cross sections. On the other hand, the absence of double-capture events can easily be understood because this reaction process is endothermic for all the incident ions and the reaction itself is not expected to occur appreciably.

For C^{2+} ions, the energy dependence of σ_1 is fairly well reproduced by the MCOB calculations, although there are rather large discrepancies in absolute values at low incident energies. As for N^{2+} and O^{2+} ions, the cross sections do not depend so strongly on the incident energy as C^{2+}. The different energy dependence observed for these ions can again be explained by the level-overlap consideration. Namely, one can see easily that the overlap of the ground state of $C^+(2s^2 2p)$ with the predominant channel $F_{1P}^{(1,0)}$ becomes smaller at lower incident energies compared to N^+ and O^+ ions. This is clearly observed in cross section data, showing σ_1 of C^{2+} to decrease more rapidly than other incident ions.

In summary, the MCOB results are in good agreement with experimental data but only at higher energies. The difference is about one order of magnitude below 10 eV/u. However, the energy dependence of the experimental values is, at least qualitatively, reproduced by our MCOB calculations. For N^{2+} and O^{2+} ions, the experimental cross sections have minima at 0.2–0.4 eV/u which are in good agreement with the MCOB results. As for the MCLZ calculations, the dominant capturing states were also found to be $2p$ states, while the agreement with experimental cross sections is worse than MCOB and the cross section minima are shifted to lower energy side than the experimental results.

At present, the influence of metastable ions in C^{2+} and O^{2+} beams on the cross section measurements is not clear.

B. C^{3+}, N^{3+}, and O^{3+}

Cross sections for $q=3$ are shown in Fig. 6. In this case, the MCLZ calculations are in fairly good agreement with the

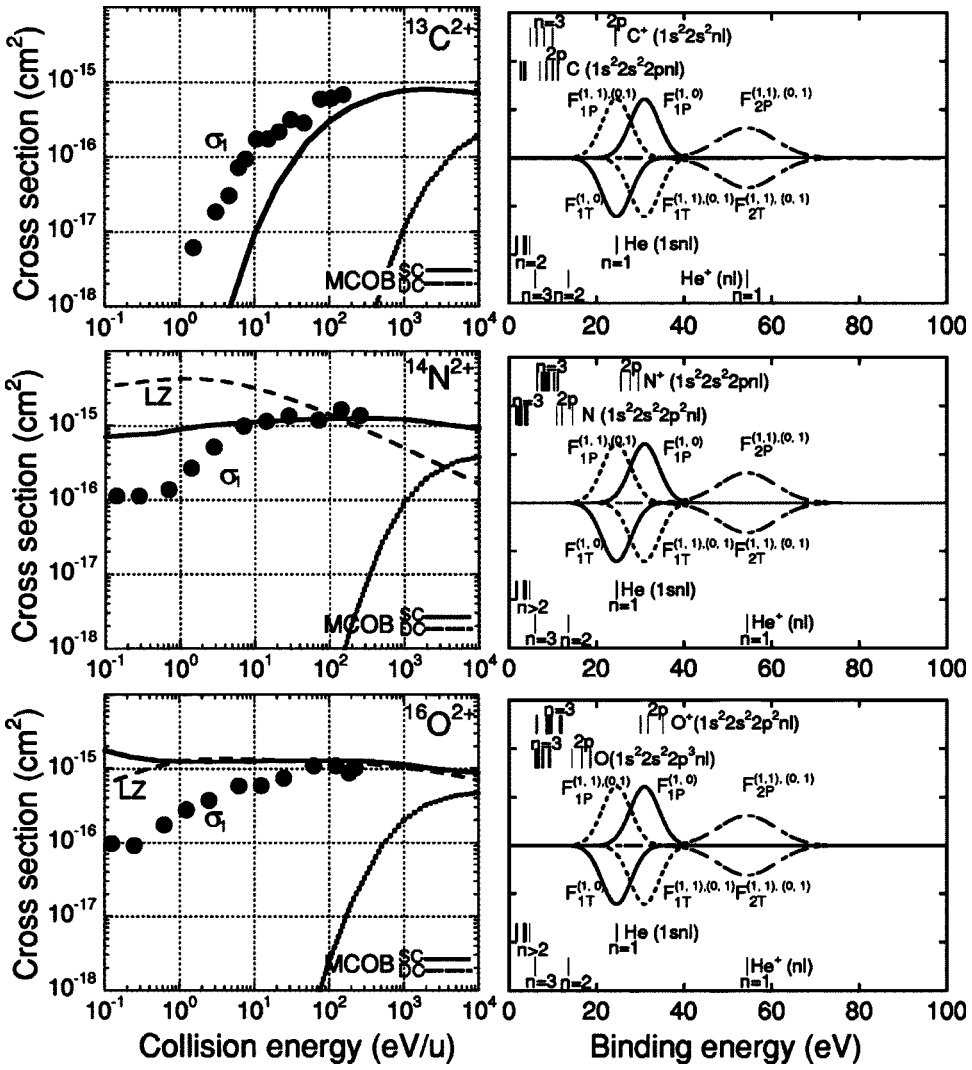

FIG. 5. Electron-capture cross sections of C^{2+}, N^{2+}, and O^{2+} in comparison with calcualted results of MCOB and MCLZ models. The energy window spectra $F_t^{(j)}(\varepsilon)$ at 100 eV/u are shown as a function of the electron binding energy ε.

experimental results of, particularly, C^{3+} and O^{3+}. Calculations were made by using doubly excited energy levels. The dominant channels were $C^{2+}(2s2p\ ^3P)$, $N^{2+}(2s2p^2\ ^2D)$, and $O^{2+}(2s2p^3\ ^3D)$, respectively. The same results were also obtained in the MCOB calculations as described below. It indicates that the projectile electron excitation is important in single-capture processes for N^{3+} and O^{3+}.

The MCOB calculations for SC can again qualitatively reproduce the experimental results. From the level-overlap consideration, the capturing state of C^{3+} is estimated to be $(2s2p)$ instead of the ground state $(2s^2)$ of C^{2+}, as seen from the energy window spectra of $F_{1P}^{(1,0)}$. This estimation is consistent with the results obtained in energy-gain experiments by Lennon *et al.* (3–18 keV) [16] and by Kimura *et al.* (3 keV/u) [17]. For N^{3+} and O^{3+} ions, there are no corresponding singly excited states but only doubly excited states as described in the previous sections. The capturing states for these ions are consequently attributed to $N^{2+}(2s2p^2)$ and $O^{2+}(2s2p^3)$, respectively.

As for double-electron-capture cross sections designated by the string $j=(1,1)$, we could measure only for N^{3+} and O^{3+} ions in the whole range of incident energy, and only two data points were obtained for C^{3+} at highest energies. For C^{3+} ions, the transition probability is expected to be small due to small level overlap in comparison with N^{3+} and O^{3+} ions. Namely, the ground state level $C^{2+}(2s^2)$ is considerably higher than the window $F_{2P}^{(1,1)}$, and simultaneously the ground state $C^+(2s^22p)$ is also located high from $F_{1P}^{(1,1)}$. At low energies the level overlap would become much smaller with decreasing width of the energy window functions. Note that the MCOB cross sections of DC are completely unrealistic as described before.

C. C^{4+}, N^{4+}, and O^{4+}

Figure 7 shows the data for $q=4$. For this charge state, the relative magnitude between SC and DC is found to be completely different for the projectile species. In particular, single capture cross sections σ_1 are considerably smaller than σ_2 for C^{4+} ions. That is mainly due to the fact that the central energy of $F_{1P}^{(1,0)}$ lies in a level-vacant zone between $n=2$ and $n=3$ of C^{3+} as seen in the figure. It indicates that the cap-

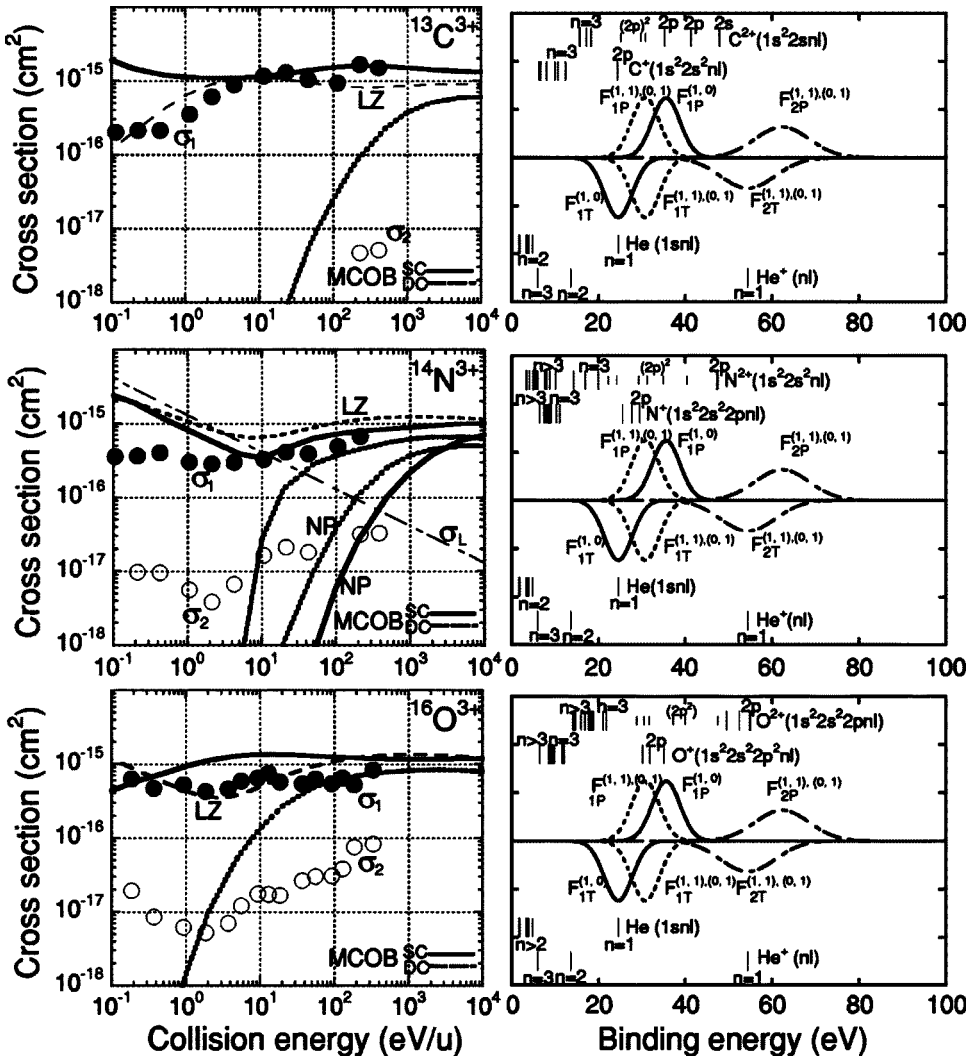

FIG. 6. Electron-capture cross sections of C^{3+}, N^{3+}, and O^{3+}. The notations are the same as Fig. 5.

tured electron is the second electron of He through a string $j=(0,1)$, as can be understood from the level-overlap between C^{3+} ($1s^22s$ and $1s^22p$) and $F_{2P}^{(0,1)}$. As the window of $F_{1P}^{(1,1)}$ covers well the levels $C^{2+}(1s^22s2p)$, the first electron of He may also be captured, resulting in the relationship of $\sigma_2 > \sigma_1$. The final stabilized configuration in double-capture process is, therefore, estimated to be $(1s^22s2p)$. It should be noted that the energy gain experiments done by Okuno *et al.* show the predominant capturing states for SC and DC to be $C^{3+}(1s^22p)$ and $C^{2+}(1s^22s^2)$, respectively [18].

As for N^{4+} and O^{4+}, the energy windows $F_{1P}^{(1,0)}$ start to cover doubly excited states formed through projectile electron promotion, so that σ_1 becomes large in comparison with the C^{4+} case. In particular this is the case for O^{4+} ions, where $F_{1P}^{(1,0)}$ well overlaps with the states $O^{3+}(1s^22p^3)$. Note, however, that the overlap of $F_{1P}^{(1,0)}$ with $O^{3+}(1s^22s^23s)$ may also be important in single capture processes. In the case of N^{4+} ions, the final state for SC and DC are estimated to be $N^{3+}(1s^22p^2)$ and $N^{2+}(1s^22p^3)$, respectively. The former state is also consistent with the results of energy gain experiments [17].

One can see that double capture cross sections σ_2 for O^{4+} are significantly small. This can also be explained from the fact of no-available levels matching with $F_{1P}^{(1,1)}$, indicating that only the second electron of He is predominantly captured. At low energies, both σ_1 and σ_2 show the Langevin type increase.

Apart from the magnitude of cross sections, the MCOB calculations can reproduce the experimentally obtained characteristics described above; i.e., the relative magnitude between σ_1 and σ_2, and energy dependence at low energies. It is noted that all these calculations include electron promotion processes, otherwise the calculated values drop rapidly with decreasing incident energy.

As for the MCLZ calculations, they are comparable with experiments only at high energies except for O^{4+} ions. The dominant channels in MCLZ calculations are $C^{3+}(1s^22p^2\mathrm{P})$ and doubly excited states of $N^{3+}(1s^22p^{21}\mathrm{S})$ and $O^{3+}(1s^22p^{22}\mathrm{P})$. Disagreements between MCLZ and experimental results are again due to the fact that the second electron of He is captured predominantly and there are no available matching levels for the first electron for C^{4+} and N^{4+} ions.

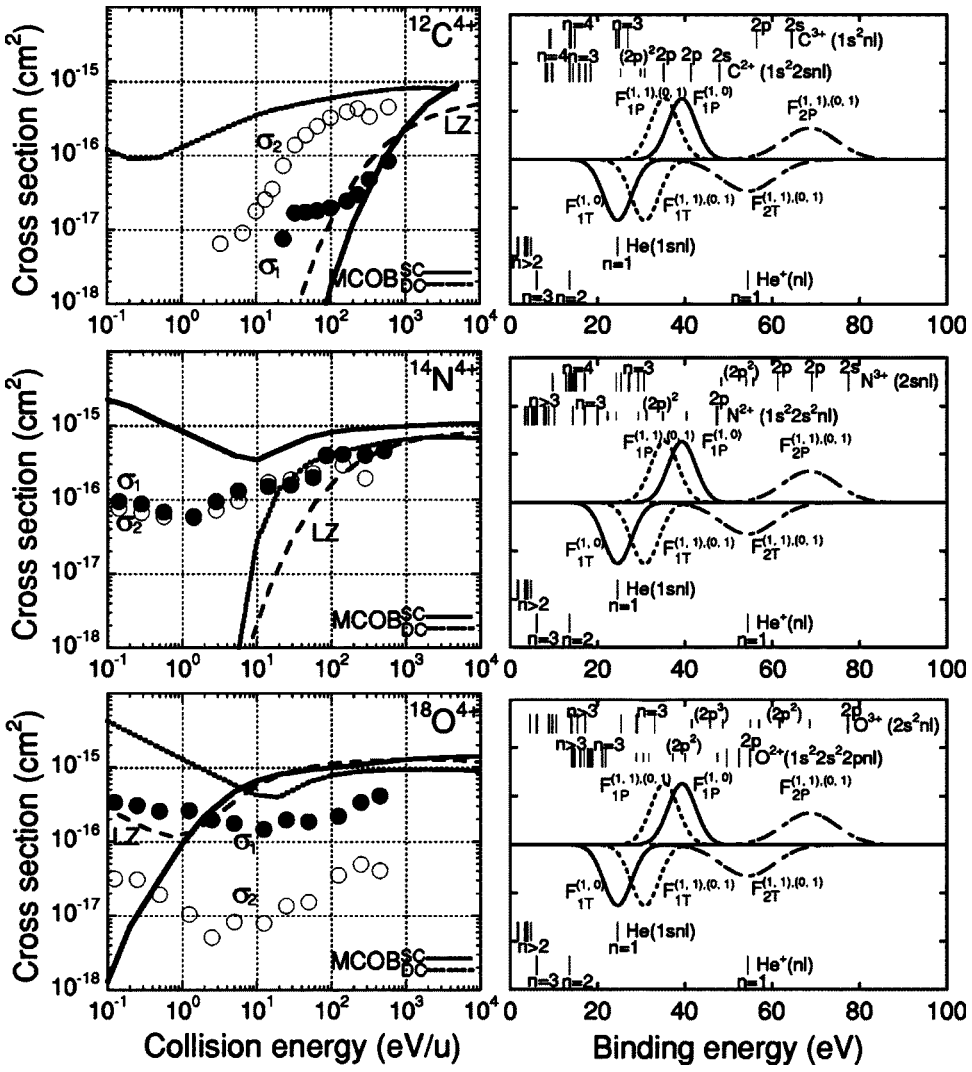

FIG. 7. Electron-capture cross sections of C^{4+}, N^{4+}, and O^{4+}. The notations are the same as Fig. 5.

D. C^{5+}, N^{5+}, and O^{5+}

Figure 8 shows the data for $q=5$. The main characteristics obtained here is large and rather energy-independent behavior of σ_1. Most cross sections are more than 10×10^{-15} cm^2 and are nearly the same irrespective of the projectile species. Apparently, this characteristic is consistent with the general feature that the single-electron capture by highly charged ions depends almost uniquely on the incident charge q but not on the projectile species [3]. Another characteristics is that the cross sections σ_2 are significantly small and reveal the Langevin type increase below a few eV/u.

The MCOB calculations of SC are in fairly good agreement with experimental values for N^{5+} ions O^{5+} ions, while for C^{5+} ions they cannot reproduce the energy dependence at low energies. This difference can also be explained from the similar level-overlap consideration. In this case, the magnitude of σ_1 is expected to be governed by the amount of overlap between $F_{1P}^{(1,0)}$ and $(3l)$ states of ions with $q=4$. Although the overlap is apparently the same for all ions, the separation in C^{4+} is larger than other projectile ions. This slightly larger separation in C^{4+} ions seems to result in the rapid decrease of cross sections at low energies, while for N^{5+} and O^{5+} the cross sections σ_1 are nearly constant values. As for double-capture cross sections, the MCOB results show again large discrepancies from the experimental values.

Although there are discrepancies between the MCOB results and experimental values, the final electronic states formed by electron capture may be summarized as follows. SC; $C^{4+}(1s3l)$, $N^{4+}(1s^23l)$, $O^{4+}(1s^22s3l)$, and DC; $C^{3+}(1s2l3l')$, $N^{3+}(1s^22l3l')$, $O^{3+}(1s^22l3l')$. It should be pointed out that the double-electron capture by C^{5+} ions forms predominantly the autoionization states $C^{3+}(1s2l3l')$. Thus, it is easily predicted that such states are stabilized to $C^{4+}(1s^2)$ via autoionization, i.e., transfer ionization in the present experiments. Actually, it is reported in other experiments [37,42] that more than 90% of DC processes are stabilized by transfer ionization. In the present work, therefore, we simply subtracted 90% from the σ_{DC} data and add them to σ_{SC}. The results are depicted by curves denoted by "TI" in

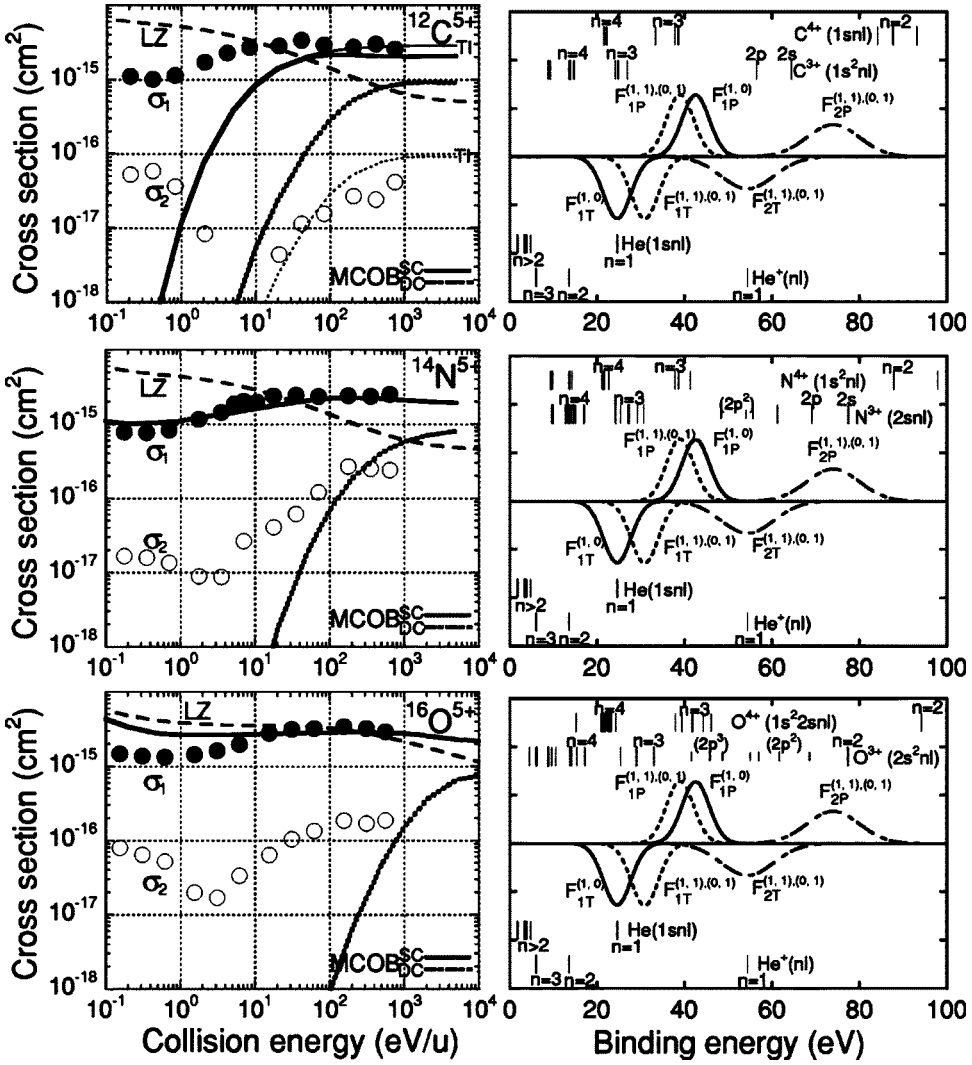

FIG. 8. Electron-capture cross sections of C^{5+}, N^{5+}, and O^{5+}. The notations are the same as Fig. 5.

the figure, showing better agreement with experimental data of both σ_1 and σ_2.

E. C^{6+}, N^{6+}, and O^{6+}

Figure 9 show the data for $q=6$. The characteristic feature observed here is that most cross sections decrease rather rapidly with decreasing incident energy and show cross section minima at about 1 eV/u. The energy dependence of the cross sections may also be explained qualitatively by the level-overlap consideration as made in the previous sections, and only brief discussion is given in this case.

From the energy window spectra, we ascribe the final electronic states as follows. SC; $C^{5+}(3l)$, $N^{5+}(1s3l)$, $O^{5+}(1s^23l)$, and DC; $C^{4+}(2l3l')$, $N^{4+}(1s2l3l')$, $O^{4+}(1s^22l3l')$. Note that the dominant channels in MCLZ calculations are $C^{5+}(3d^2\mathrm{D})$, $N^{5+}(1s3p^1\mathrm{P})$ and $O^{5+}(1s^23d^2\mathrm{D})$. These estimations are in good agreement with the results of energy gain spectroscopy experiments [18,19] reporting $n=3$ as the predominant capturing states in single-capture collisions. As for double-electron capture processes, electronic states given above are apt to stabilize via autoionization. It is interesting to note that similar electronic configurations are identified in electron spectroscopy experiments by Stolterfoht *et al.* [43]. They also report that two electrons are captured with sufficiently large probabilities into asymmetric doubly excited states of $(2lnl)$ with $n>10$.

Finally, the MCOB calculations also decrease with decreasing incident energy but more rapidly compared to experimental values. This is again attributed to nonoverlap characteristics of energy levels under consideration.

V. CONCLUSION

Single- and double-electron capture cross sections have been measured for C^{q+}, N^{q+}, and O^{q+} $(q=2-6)$ ions in He at incident energies of $(1.0-1800)q$ eV. In a high energy range, the present data are reasonably comparable with other previous high energy data. As general characteristics, the cross sections for endothermic reactions were found to decrease rapidly with decreasing incident energy and those for exothermic reactions to reveal cross section minima at a few eV/u and vary as v^{-1} below this energy.

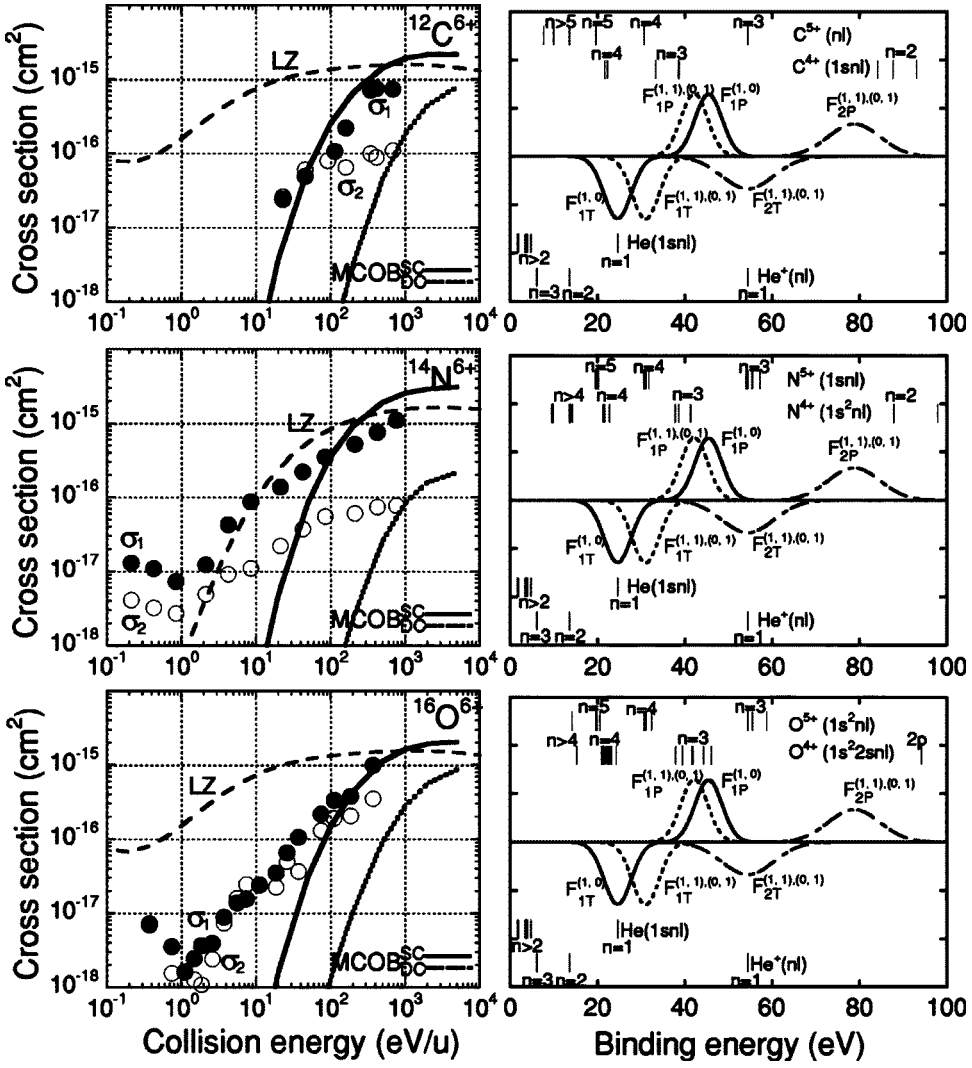

FIG. 9. Electron-capture cross sections of C^{6+}, N^{6+}, and O^{6+}. The notations are the same as Fig. 5.

To account for these characteristics, we carried out calculations on the basis of the extended classical overbarrier model [6,7] and on the multichannel Landau-Zener model [9,10]. We used the induced dipole attractive potential which is considered as a typical potential form in slow ion-atom collisions. In addition to the critical nuclear distances r_t at which a target electron belongs to both projectile and target particles, we also calculated the nuclear distance r_{orb} at which the incident ion starts orbiting, in order to obtain velocity dependent cross sections. Furthermore, the projectile excitation accompanying electron-capture events is taken into consideration in our calculations. As a whole, the present calculations can reproduce fairly well the experimental cross sections as described in detail in Sec. IV. From level-overlap considerations, we could successfully estimate the predominant capturing states both for single- and double-electron-capture processes. Most of our estimations are in good agreement with other more direct experiments like energy-gain spectroscopy and electron spectroscopy. Particular success of our model calculations is that the energy dependence of the experimental cross sections including v^{-1} behavior at low velocities is reasonably reproduced. In conclusion, more exact interaction potentials such as an induced dipole potential used in this work and additional excitation processes like projectile electron promotion should inevitably be taken into consideration to account for the experimental electron-capture cross sections at very low incident energies.

ACKNOWLEDGMENTS

This work was supported in part by a Grant-in-Aid for Scientific Research from the Ministry of Education, Culture, Sports, Science and Technology of Japan.

[1] H. Tawara, T. Kato, and Y. Nakai, At. Data Nucl. Data Tables **32**, 235 (1985).
[2] R. K. Janev, R. A. Phaneuf, and H. Hunter, At. Data Nucl. Data Tables **40**, 249 (1988).
[3] A. Muller and E. Salzborn, Phys. Lett. **62A**, 391 (1977).
[4] T. Iwai *et al.*, Phys. Rev. A **26**, 105 (1982).
[5] H. Ryufuku, K. Sasaki, and T. Watanabe, Phys. Rev. A **21**, 745 (1980).
[6] A. Bárány *et al.*, Nucl. Instrum. Methods Phys. Res. B **9**, 397 (1985).
[7] A. Niehaus, J. Phys. B **19**, 2905 (1986).
[8] B. Bransden and M. McDowell, *Charge Exchange and the Theory of Ion-Atom Collisions* (Clarendon Press, Oxford, 1992).
[9] R. E. Olson and A. Salap, Phys. Rev. A **14**, 579 (1976).
[10] A. Salop and R. E. Olson, Phys. Rev. A **13**, 1312 (1979).
[11] K. Okuno, J. Phys. Soc. Jpn. **55**, 1504 (1986).
[12] K. Suzuki, K. Okuno, and N. Kobayashi, Phys. Scr., T **T73**, 172 (1997).
[13] K. Ishii, K. Okuno, and N. Kobayashi, Phys. Scr., T **T80**, 176 (1999).
[14] K. Ishii *et al.*, Phys. Scr., T **T92**, 332 (2001).
[15] G. Gioumousus and D. Stevenson, J. Chem. Phys. **29**, 294 (1958).
[16] M. Lennon, R. W. McCullough, and H. B. Gilbody, J. Phys. B **16**, 2191 (1983).
[17] M. Kimura *et al.*, J. Phys. B **15**, L851 (1982).
[18] K. Okuno *et al.*, Phys. Rev. A **28**, 127 (1983).
[19] A. Ohtani *et al.*, J. Phys. B **15**, L533 (1983).
[20] WWW homepage of the NIST Atomic Spactra Database. (http://physics.nist.gov/).
[21] K. Taulbjerg, J. Phys. B **19**, L367 (1986).
[22] K. Okuno, K. Soejima, and Y. Kaneko, Nucl. Instrum. Methods Phys. Res. B **53**, 387 (1991).
[23] K. Soejima *et al.*, J. Phys. B **25**, 3009 (1992).
[24] E. Unterreiter, J. Schweinzer, and H. Winter, J. Phys. B **24**, 1003 (1991).
[25] J. B. Hasted and R. A. Smith, Proc. R. Soc. London, Ser. A **235**, 354 (1956).
[26] L. D. Gardner, Phys. Rev. A **20**, 766 (1979).
[27] J. F. Castillo *et al.*, J. Phys. B **27**, 5027 (1994).
[28] E. C. Montenegro G. M. Sigaud, Phys. Rev. A **45**, 1575 (1992).
[29] W. S. Melo *et al.*, Phys. Rev. A **60**, 1124 (1999).
[30] D. Dijkkamp *et al.*, J. Phys. B **18**, 4763 (1985).
[31] D. H. Crandall, M. L. Mallory, and D. C. Kocher, Phys. Rev. A **15**, 61 (1977).
[32] M. Kimura and R. E. Olson, J. Phys. B **17**, L713 (1984).
[33] W. Fritsch and C. D. Lin, Phys. Rev. A **54**, 4931 (1996).
[34] J. P. Hansen and K. Taulbjerg, Phys. Rev. A **47**, 2987 (1993).
[35] T. Ohyama-Yamaguchi, J. Phys. Soc. Jpn. **56**, 1693 (1986).
[36] Y. S. Gordeev *et al.*, Phys. Rev. Lett. **50**, 1842 (1983).
[37] E. Y. Kamber *et al.*, Phys. Rev. A **60**, 2907 (1999).
[38] T. K. McLaughlin *et al.*, J. Phys. B **26**, 3871 (1993).
[39] J. P. M. Beijers, R. Hoekstra, and R. Morgenstern, Phys. Rev. A **49**, 363 (1994).
[40] M. G. Suraud *et al.*, J. Phys. B **18**, 4763 (1991).
[41] T. Shimakura *et al.*, J. Phys. B **20**, 201801 (1987).
[42] H. Zhang *et al.*, Phys. Rev. A **60**, 3694 (1999).
[43] N. Stolterfoht *et al.*, Phys. Rev. Lett. **57**, 74 (1986).